

Highly efficient visible light mediated photocatalytic degradation of alizarin yellow dye and antibacterial activity by polyaniline/reduced graphene oxide anchored to NiFe double layered hydroxide

S. Yadav ^a, A. Jilani ^b, A. Prajapati ^a, S. Sachan ^a, R. S. Yadav ^a, M. Oves ^c,
S. K. Chaurasia ^d, A. Yadav ^e, M. O. Ansari ^b, P. Kumar ^{a,*}

^a Functional Materials Laboratory, Department of Chemistry Prof. Rajendra Singh (Rajju Bhaiya), Institute of Physical Sciences for Study and Research, Veer Bahadur Singh Purvanchal University, Jaunpur-222003, Uttar Pradesh, India

^b Center of Nanotechnology, King Abdul-Aziz University, Jeddah 21589, Saudi Arabia

^c Center of Excellence in Environmental Studies, King Abdul-Aziz University, Jeddah 21589, Saudi Arabia

^d Centre for Nanoscience & Technology, Prof. Rajendra Singh (Rajju Bhaiya), Institute of Physical Sciences for Study and Research, Veer Bahadur Singh Purvanchal University, Jaunpur-222003, Uttar Pradesh, India

^e Green Laboratory, Department of Chemistry, Ewing Christian College (University of Allahabad) Prayagraj-211003, Uttar Pradesh, India

Herein nickel-iron double layered hydroxide (NiFe-DLH) was prepared by co-precipitation and further binary rGO@NiFe-DLH and ternary Pani/rGO@NiFe-DLH composite was synthesized by doping NiFe-DLH with reduced graphene oxide (rGO) and rGO plus polyaniline (Pani) respectively by hydrothermal methodology. Upon visible light exposure the ternary composite showed superior degradation of alizarin yellow R (AYR) dye in comparison to NiFe-DLH and rGO@NiFe-DLH. The X-ray diffraction, scanning electron microscopy and photoluminescence spectroscopy were used to analyze Pani and rGO integration into the NiFe-DLH structure. The degradation efficiency of AYR dye at various conditions was employed to evaluate the photocatalytic performance of the ternary Pani/rGO@NiFe-DLH composite. A significant enhancement in the photocatalytic efficiency of ternary composite as compared to NiFe-DLH and rGO@NiFe-DLH was observed. The ternary composite showed exceptional durability and reusability throughout 10 cycles of degradation. Apart from this, antibacterial potency of the nanocomposite against gram-negative bacterium *E. coli* was also studied, which indicated significant growth inhibition of *E. coli* in liquid culture.

(Received February 16, 2025; Accepted June 10, 2025)

Keywords: Reduced graphene oxide, Polyaniline, Double layer hydroxide, Photocatalytic degradation

1. Introduction

The textile industry's direct release of the highly toxic, non-biodegradable and chemically stable azo dyes into water bodies is the main cause of water pollution, which affects aquatic life in the water ecosystem as well as humans, due to their mutagenic, carcinogenic, and teratogenic nature [1]. Due to their non-biodegradable and chemically stable nature these dyes persist in the environment for long times and thus are often responsible for large number of diseases such as heart issues, lung cancer, chromosomal abnormalities, neurotoxicity, skin and respiratory issues in humans [2]. By altering metabolism in living beings, they cause major harm to aquatic life and reduce the amount of sunlight that reaches the water [3,4]. As a result, it becomes evident to treat dyes contaminated waste before releasing it into the main water stream.

The water-soluble anionic dye known as alizarin yellow R (AYR) is often used as pH indicator and as a biological stain in the chemical analysis processes within the textile industry

* Corresponding authors: pkchemistry.2009@gmail.com

<https://doi.org/10.15251/DJNB.2025.202.609>

dyeing works. They are resistant to deterioration because of their complex aromatic structure, which gives them long-lasting stability[5]. Additionally, they exhibit significant persistence in the aquatic ecosystem due to their high chemical stability and are non-biodegradable in both aerobic and anaerobic environments[6]. Their toxicity and carcinogenicity are high; hence they need to be eliminated before being released into the major water streams. Several processes such as coagulation [7], precipitation by chemicals [8], adsorption by porous or functionalized materials [9], membrane filtration [10], and electrochemical reactions [11] have been widely used to remove AYR from the environment. Although these processes break down the dyes into innocuous final products, the creation of poisonous sludge and dangerous secondary pollutants poses a major environmental risk [12].

Therefore, it is necessary to utilize water treatment technologies for dye degradation that are efficient, economical, and sustainable. Photocatalysis has become a viable substitute for the breakdown of poisonous chemical molecules and dangerous water-soluble dyes[13]. The process of photocatalysis involves the breakdown of dyes molecules in the presence of photocatalysts when exposed to the light source [14]. Photo-generation of electron-hole occurs on the surface of photocatalysts on exposure to radiation [15]. The surface of the photocatalyst absorbs light energy exceeding its band gap threshold which excites valence band electrons into conduction bands thus creating holes behind [16]. Dissolved oxygen molecules in the water solution interact with holes and electrons from photo-generation to generate free radical species ($\bullet\text{OH}$, $\text{O}_2\bullet^-$ and $\bullet\text{OOH}$) [17]. The formed reactive free radical species attacks organic pollutants found within the water to generate low molecular weight, harmless, biodegradable products [18].

Since the discovery of photocatalysis, a lot of semiconductors-based catalysts comprising of TiO_2 , ZnO , MnO_2 , SnO_2 , AgX ($\text{X}=\text{Cl}$, Br , I), etc. have been widely explored for mineralization of organic water pollutants [19-21]. Recently double layered hydroxide (DLH), also referred to as hydrotalcite-like compounds with chemical formula $[\text{M}^{2+}_{1-x}\text{M}^{3+}_x(\text{OH})_2]^{x+}(\text{An}^-)_{x/n}\cdot m\text{H}_2\text{O}$ where M is metal cation, An^- is organic/inorganic anions and m is water of crystallization have shown huge potential for photocatalytic mineralization of organic pollutants [22-26].

Metal-salen complexes where metal is Co or Ni in combination with ZnCr-DLH showed highly efficient Rhodamine B mineralization which significantly exceeded commercial catalysts [27]. Several recent studies confirmed that NiFe-DLH or modified NiFe-DLH exhibited photocatalytic activity toward polluted water containing dyes [28]. However, more research is required to boost DLH-based photocatalysts powered by visible light into suitable semiconductor materials. The extended π -conjugated structures of conducting polymers such as polyaniline (Pani) or polypyrrole and carbon materials such as graphene oxide (rGO), have garnered a lot of interest as photocatalytic absorbers that can enhance semiconductor photo-response [29–31]. Inspired by the aforementioned study, in this work Pani/rGO@FeNi-DLH ternary composite was synthesized and tested for the photocatalytic activity by degrading AYR dye under visible light as well as studying its antibacterial potency against gram negative *E. coli* bacteria.

2. Experimental

2.1. Materials required

Ferric nitrate nanohydrate ($\text{Fe}(\text{NO}_3)_3\cdot 9\text{H}_2\text{O}$) 98% SRL, nickel nitrate hexahydrate ($\text{Ni}(\text{NO}_3)_2\cdot 6\text{H}_2\text{O}$) 99% SRL, sodium hydroxide pellets (NaOH) 98% SRL, aniline, N-methyl-2-pyrrolidone (NMP), hydrochloric acid (35%), phosphoric acid (85%), potassium persulfate, potassium permanganate, sulfuric acid (98%), hydrogen peroxide (30%), ammonia solution and graphite powder were used. *Escherichia coli* bacterial strain was cultured in Luria-Bertani (LB) broth at 37 °C with continuous shaking (150 rpm) until reaching the mid-log phase ($\text{OD}_{600} \sim 0.6$).

2.2. Method

For morphological analysis, field emission scanning electron microscope (FESEM) (model: JEOL, JSM-7600F, FESEM, Tokyo, Japan) was used, while the elemental mapping was done with an energy dispersive X-ray spectrometer (EDS) from Oxford Instruments, Oxfordshire, UK. The surface chemical composition and structure of Pani/rGO@NiFe-DLH composite were investigated

by using a monochromatized Al K α X-ray source (λ 1/4 1486.6 eV) and X-ray photoelectron spectroscopy (XPS) were done with ESCALAB 250 from thermal fisher scientific, Warrington, UK. The rate of charge recombination, photogenerated hole and free electrons during the photocatalytic processes was investigated by photoluminescence spectroscopy.

2.2.1. Synthesis of Pani/rGO@NiFe-DLH composites

The synthesis of GO and Pani stock solution can be seen elsewhere [32]. The synthesis of NiFe-DLH was done by simple co-precipitation method. In a typical process, 2.61 gram of nickel nitrate and 1.21 grams of Iron(III) nitrate nonahydrate were dissolved in separate 50 mL beaker and stirred for 30 min to get a homogenous solution. There after both solutions were mixed and pH 9 was maintained with the help of NaOH (1M) solution. The stirring was continued for 24h, resulting in the precipitation of NiFe-DLH which was separated by centrifugation, washed multiple times with water and ethanol and subsequently dried at 80 °C overnight. For the synthesis of rGO@NiFe-DLH composite, the obtained NiFe-DLH was dispersed in 50 mL water and 10 mL of GO (5mg/mL) was added to it. The whole dispersion was charged into Teflon line hydrothermal reactor and heated at 160 °C for 16h to get rGO@NiFe-DLH. Thus, obtained rGO@NiFe-DLH was multiple time with water and ethanol and finally dried at 80 °C overnight. For the synthesis of ternary Pani/rGO@NiFe-DLH, a 500 μ l of Pani stock solution was added along with GO solution and rest of the procedure was same as in the case of rGO@NiFe-DLH composite.

2.2.2. Photocatalytic study

The synthesized materials NiFe-DLH, rGO@NiFe-DLH and Pani/rGO@NiFe-DLH was evaluated for the performance of photocatalytic activity by using AYR as a model pollutant under visible light irradiation. The photocatalytic experiment was conducted in a 100 mL reaction vessel containing 50 mL of 20 ppm AYR solution with an optimized photocatalyst dose of 0.1 g/L. The suspension was magnetically stirred for 30 minutes in the absence of visible light for adsorption-desorption equilibrium between AYR molecules and catalyst surface.

The 150 W halogen lamp was used as a visible light source and after irradiation and during degradation, 3 mL aliquots were withdrawn from suspension after every 15-minute intervals for up to 90 minutes. The eliminate photocatalyst particles from each sample, a 0.45 μ m syringe filter paper was used. The residual concentration of AYR in the filtrate was determined by employing a UV-Vis spectrophotometer to measure the absorbance at its characteristic wavelength (420 nm). The formula (1) was used to calculate photocatalytic degradation efficiency of the catalyst:

$$\text{Degradation}(\%) = \left(\frac{C_o - C_t}{C_o} \right) 100 \quad (1)$$

The formula (2) used to calculate the rate constant (k) of photocatalytic reaction.

$$\ln\left(\frac{C_t}{C_o}\right) = -kt \quad (2)$$

To confirm the contributions of photocatalysis, control experiments were conducted under the identical circumstances without light and photocatalyst. The effect of the individual components (NiFe-DLH, rGO@NiFe-DLH and Pani/rGO@NiFe-DLH) on photocatalytic activity was also evaluated for comparison.

2.2.3. Antimicrobial activity assay

For liquid inhibition assays, 100 μ L of *E. coli* culture was treated with each nanocomposite and incubated at 37 °C for 24 hours. Bacterial growth was measured by using a micro plate reader at OD600.

2.2.4. Agar diffusion assay

For zone of inhibition studies, 50 μ L of *E. coli* suspension was spread on LB agar plates, and wells were filled with 100 μ L of each composite. Plates were incubated at 37 °C for 24 hours, and inhibition zones were measured.

2.2.5. Data analysis

Experiments were performed in triplicate, and results were analysed using one-way ANOVA for statistical significance.

3. Result and discussion

3.1. XRD analysis

The XRD analysis of NiFe-DLH, rGO@NiFe-DLH and Pani/rGO@NiFe-DLH is presented in Figure 1. For NiFe-DLH, the peaks at 11.30, 23.01, 34.6 and 60.22 2θ shows successful synthesis of NiFe-DLH [33]. The XRD pattern of rGO@NiFe-DLH composites corresponds to the hexagonal NiFe-DLH, with no distinctive graphite peak seen. This result shows that the restacking graphene sheets is successfully inhibited, as seen by total graphite exfoliation in the rGO@NiFe-DLH composite [34]. Additional research has demonstrated that if the regular stacks of graphite oxide or graphite are harmed by exfoliation, the diffraction peaks of these materials would weaken or even vanish [35–37]. In the Pani/rGO@NiFe-DLH ternary composites, Pani peak is not distinct due to its low concentration and amorphous nature.

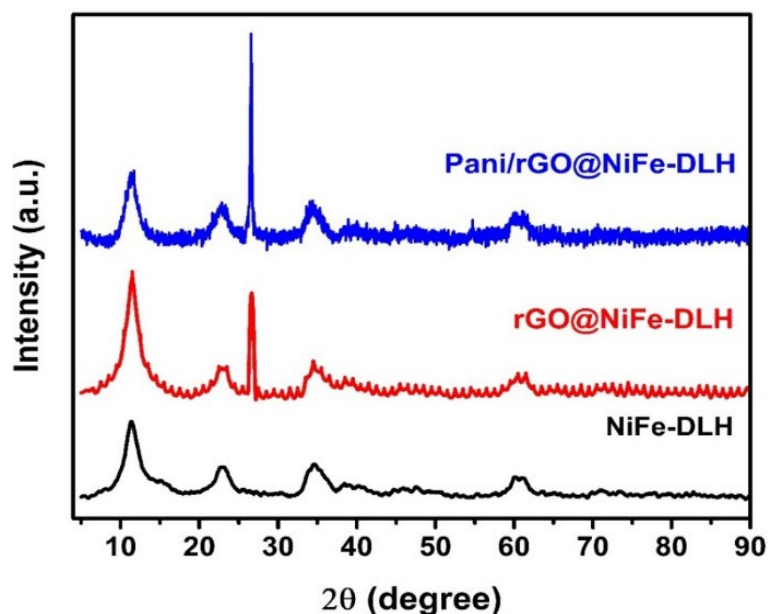


Fig. 1. XRD of NiFe-DLH, rGO@NiFe-DLH and Pani/ rGO@NiFe-DLH.

3.2. Morphology analysis

The morphology of base material and ternary composite were investigated by using SEM and elemental composition were investigated by EDS that is shown in Figure 2. Figure 2a clearly shows the big blocks of NiFe-DLH while in rGO@NiFe-DLH (Figure 2b), apart from NiFe-DLH, the distinct rGO sheets is visible. The morphology of Pani/rGO@NiFe-DLH (Figure 2c) is similar as in rGO@NiFe-DLH due to the low content of Pani. The presence of C, O, N, Fe and Ni in the EDS spectra suggests the efficacy of the synthesis methodology (Figure 2d).

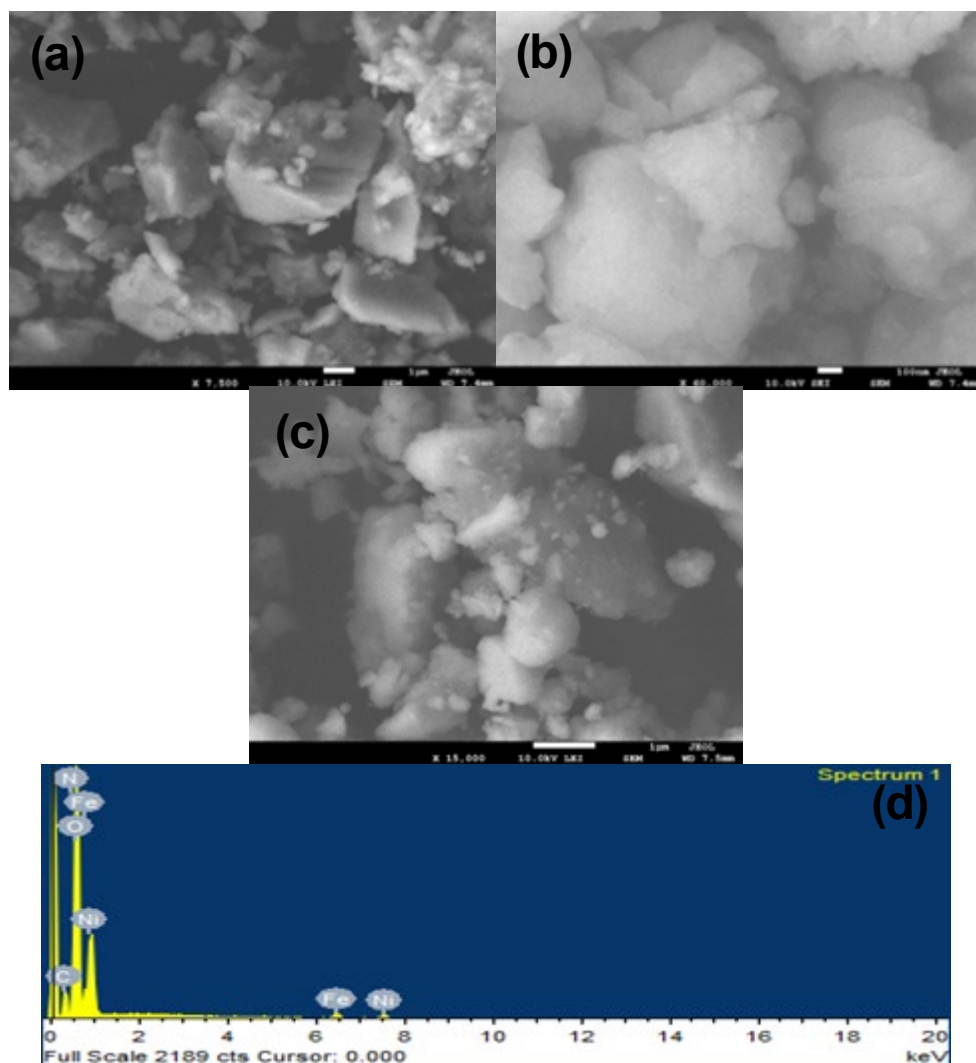


Fig. 2. SEM image of (a) NiFe-DLH, (b) rGO@NiFe-DLH (c) Pani/rGO@NiFe-DLH and (d) EDS of Pani/rGO@NiFe-DLH ternary composites.

3.3. Charge recombination behavior

The photoluminescence (PL) spectra provide insights into the charge recombination behavior of the synthesized NiFe-DLH and its composites, directly correlating to their photocatalytic efficiencies. Among the tested materials, NiFe-DLH exhibited the highest PL intensity (Figure 3), indicating a high rate of charge carrier recombination, which limits the availability of electrons and holes for initiating photocatalytic reactions. This high recombination rate is consistent with its lower photocatalytic activity and degradation efficiency for AYR [38]. In contrast, the PL intensity of rGO@NiFe-DLH is significantly reduced, suggesting that the incorporation of rGO effectively suppresses charge recombination by acting as an electron acceptor and promoting charge transfer [39]. This reduction in charge recombination contributes to the enhanced generation of reactive oxygen species, thereby improving the degradation efficiency of AYR. The Pani/rGO@NiFe-DLH composite shows the lowest PL intensity among all tested materials, reflecting the most efficient charge separation and the lowest charge recombination rate. The synergistic interaction between Pani and rGO enhances electron transfer and prolongs the lifetime of charge carriers, promoting a greater activity of photocatalysis. The suppressed PL intensity in the ternary composite directly correlates with its superior photocatalytic degradation of AYR, as efficient charge separation ensures the generation of more reactive species responsible for breaking down dye molecules.

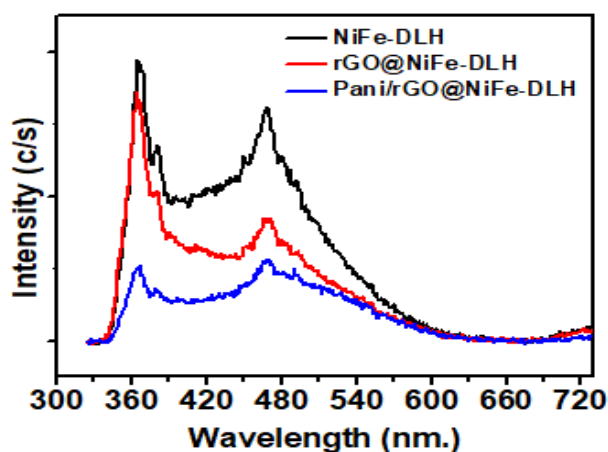


Fig. 3. PL spectra for NiFe-DLH, rGO@NiFe-DLH, and Pani/rGO@NiFe-DLH.

3.4. Band gap analysis

The energy band gaps of the ternary composites was determined by using the adsorption spectra and Tauc plot method. Pure NiFe-DLH exhibited a band gap of 2.16 eV (Figure 4a), which is consistent with the limited visible light absorption and suboptimal photocatalytic activity observed in this material. Upon the incorporation of rGO into NiFe-DLH, the band gap decreased to 2.06 eV (Figure 4b).

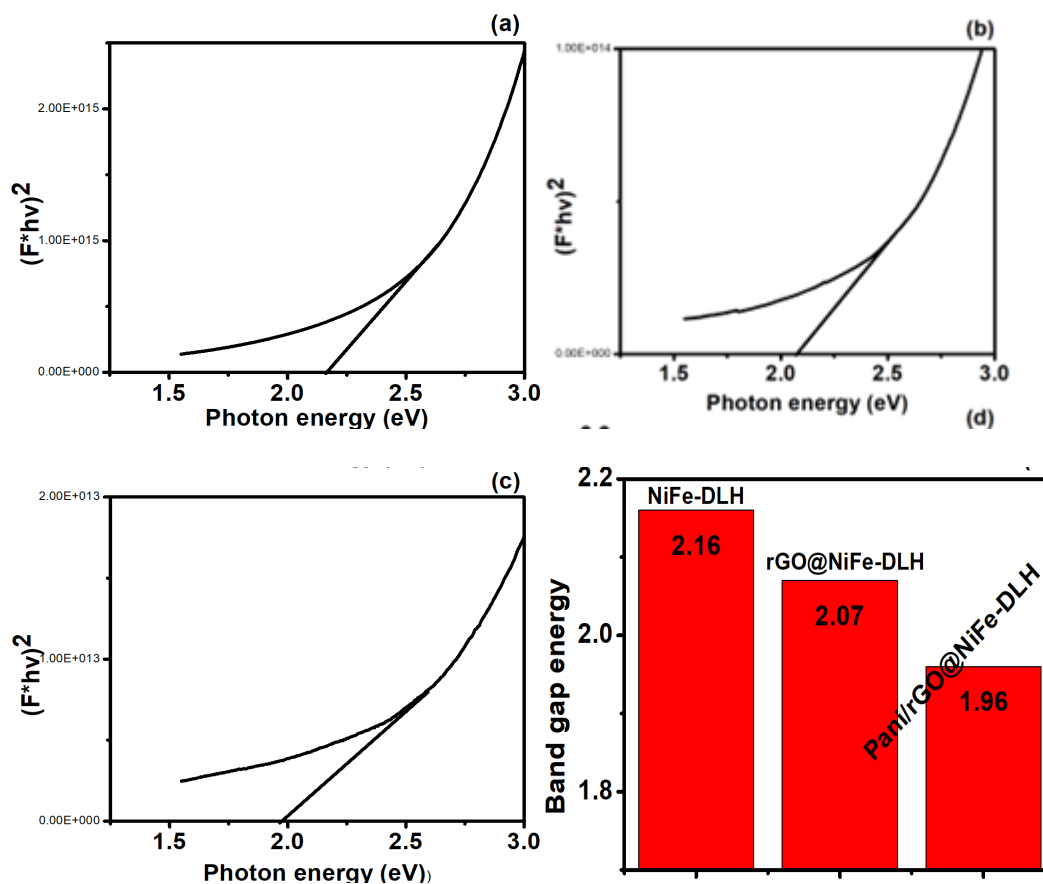


Fig. 4. Band gap analysis for (a) NiFe-DLH, (b) rGO@NiFe-DLH, (c) Pani/rGO@NiFe-DLH and (d) band gap presentation.

This reduction can be attributed to the electronic interactions between rGO and NiFe-DLH. The incorporation of rGO enhances the delocalization of electrons, thereby narrowing the band gap and enabling better absorption of visible light. The photocatalytic efficiency is further enhanced by the reduced charge carrier recombination caused by rGO which functions as an electron sink. Once Pani was added to the rGO@NiFe-DLH composite, the band gap further decreased to 1.96 eV (Figure 4c).

The Pani, which has a tiny inherent band gap, greatly increases the composite's absorption range into the visible spectrum. The synergistic combination of Pani, rGO, and NiFe-DLH allows for effective charge transfer and separation, which contributes to the ternary composite's increased photocatalytic activity. The decreased band gap enhances photon absorption under visible light irradiation, encouraging the formation of reactive oxygen species that promote AYR degradation. The progressive reduction in band gap from 2.16 eV (NiFe-DLH) to 1.96 eV (Pani/rGO@NiFe-DLH) (Figure 4d) demonstrates the effectiveness of incorporating rGO and Pani in modifying the electronic structure of NiFe-DLH.

3.5. Photocatalytic degradation of AYR

In this study, the photocatalytic degradation of AYR was evaluated using three different photocatalysts, NiFe-DLH, rGO@NiFe-DLH, and Pani/rGO@NiFe-DLH. The photocatalytic activity was monitored at 15-minute intervals over a 90-minute period, with degradation efficiencies of 85, 70, and 40%, respectively (Figure 5a-b). The calculated reaction rate constants were $0.005764 \text{ min}^{-1}$ for NiFe-DLH, $0.013377 \text{ min}^{-1}$ for rGO@NiFe-DLH, and $0.021621 \text{ min}^{-1}$ for Pani/rGO@NiFe-DLH, reflecting the trend in degradation efficiency (Figure 5c).

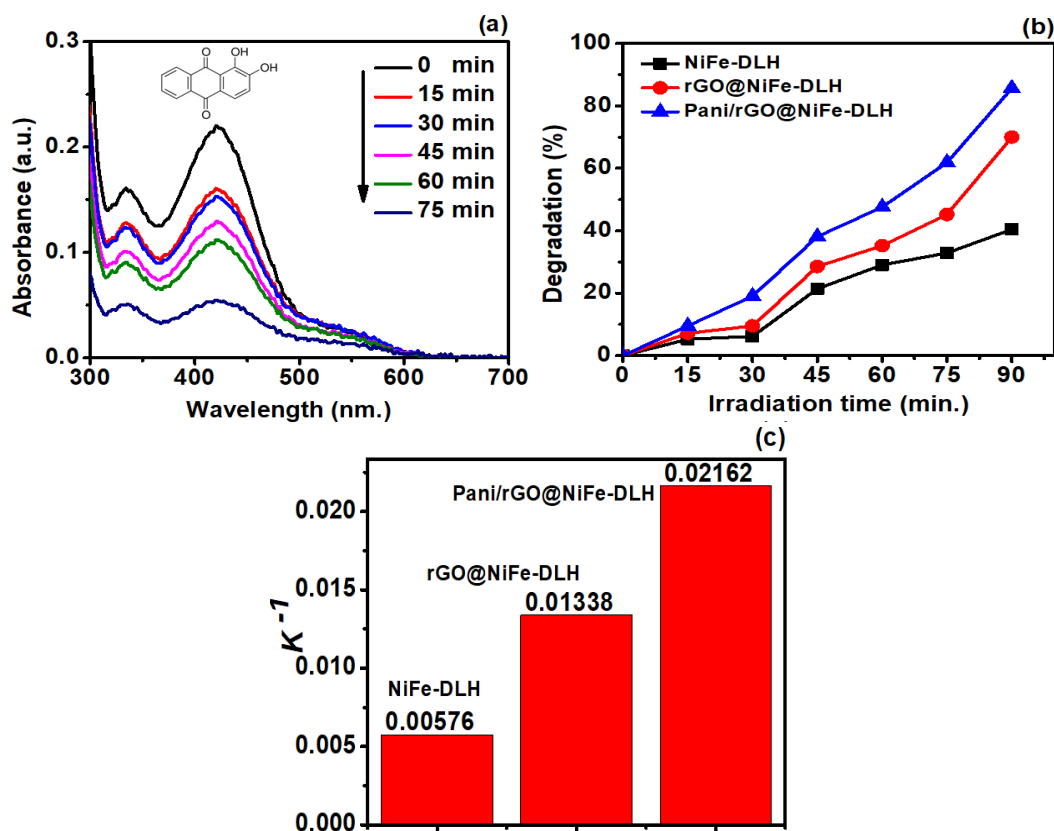


Fig. 5. Degradation of AYR (a) Adsorption spectra of Pani/rGO@NiFe-DLH (b) percentage degradation, (c) reaction rate constant of NiFe-DLH, rGO@NiFe-DLH, and Pani/rGO@NiFe-DLH.

The pure NiFe-DLH exhibited the lowest performance, which can be attributed to its relatively high bandgap and limited visible light absorption, resulting in poor photocatalytic activity[40]. The quick recombination of photogenerated electron-hole pairs in NiFe-DLH further contributed to its suboptimal efficiency[41]. Despite the layered structure of NiFe-DLH facilitating ion exchange and adsorption, the absence of effective charge separation mechanisms limits its photocatalytic potential under visible light. This limitation is evident in its low reaction rate constant of $0.005764 \text{ min}^{-1}$, indicating sluggish degradation kinetics.

The incorporation of rGO to NiFe-DLH significantly improved the degradation efficiency, increasing it to 70%, with a corresponding reaction rate constant of $0.013377 \text{ min}^{-1}$. This enhancement can be attributed to rGO role as an electron sink, which reduces the recombination of photogenerated charge carriers [42]. The rGO increases the lifespan of reactive species like hydroxyl radicals ($\bullet\text{OH}$) and superoxide radicals ($\text{O}_2\bullet^-$) by facilitating electron transfer from NiFe-DLH's conduction band. These reactive species play an essential role in the degradation of AYR [42]. Additionally, the incorporation of rGO contributes to the reduction in the bandgap of NiFe-DLH, allowing for better utilization of visible light, which is another reason for the enhanced degradation of AYR [43]. The enhanced electron mobility provided by rGO mirrors the behavior observed in photocatalysts like $\text{G-TiO}_2@\text{Fe}_3\text{O}_4$, where the incorporation of carbon based materials facilitates electron transfer and reduces the rate of charge recombination [44].

The highest degradation efficiency of 85% was observed for the ternary Pani/rGO@NiFe-DLH composite, with a reaction rate constant of $0.021621 \text{ min}^{-1}$, the highest among the prepared photocatalysts. This superior performance is due to the synergistic effect between Pani and rGO, where Pani extends the visible light absorption range and enhances charge separation [45]. Pani, a conducting polymer with a narrow bandgap, efficiently transfers photogenerated electrons to rGO, which subsequently shuttles them to the conduction band of NiFe-DLH, sustaining prolonged electron availability. This extension of light absorption into the visible region is a key factor in the improved photocatalytic activity, as Pani reduces the overall bandgap of the composite. The decreased bandgap allows for improved photon absorption under visible light, boosting the production of reactive oxygen species responsible for dye degradation. Pani plays a similar role to graphite in TiO_2 -based catalysts, helping to reduce bandgaps and improve charge separation efficiency[46].

3.6. Effect of AYR concentration

The effect of AYR dye concentration on the photocatalytic degradation ability of Pani/rGO@NiFe-DLH was investigated using four different concentrations of AYR: 20, 30, 40, and 50 ppm. The highest degradation efficiency of approximately 85% was achieved at 20 ppm after 90 minutes of visible light irradiation (Figure 6a).

At 30 ppm, the degradation efficiency decreased to 79%, and further reduction was observed at 40 ppm (76%) and 50 ppm (70%). The decrease in catalytic efficiency with increasing dye concentration can be attributed to several factors. At lower concentrations (20 ppm), there is a more favorable balance between dye molecules and active sites on the photocatalyst surface, leading to optimal interaction and efficient generation of reactive species like hydroxyl radicals ($\bullet\text{OH}$) and superoxide radicals ($\text{O}_2\bullet^-$) [47]. These reactive species are key to the degradation process, and their generation is maximized at the optimal dye concentration.

As the dye concentration increases, there is an excess of dye molecules that occupy the catalyst surface which limits its exposure to light [48]. This limits the production of photogenerated charge carriers, as the catalyst surface becomes saturated, leading to reduced efficiency in charge separation and diminished photocatalytic activity. Furthermore, at higher concentrations (40 and 50 ppm), the excess dye molecules also absorb a significant part of the incident light, reducing the photon flux available to excite the catalyst, thus further decreasing the generation of reactive species.

These results suggest that while Pani/rGO@NiFe-DLH is highly efficient at lower dye concentrations, there is an optimal concentration range beyond which the photocatalytic performance diminishes.

3.7. Reusability and stability of the Pani/rGO@NiFe-DLH

To assess reusability and the stability of the Pani/rGO@NiFe-DLH photocatalyst, a cyclic degradation test was performed at a fixed dye concentration of 20 ppm (Figure 6b). After 10 consecutive cycles, the degradation efficiency remained relatively high, with a value of approximately 81%. This indicates that the catalyst exhibits good stability and maintains a significant portion of its photocatalytic activity over multiple cycles. The slight decrease in degradation efficiency compared to the initial cycle (85%) may be attributed to factors such as the accumulation of degradation intermediates on the catalyst's surface, which could hinder the active sites and reduce the overall catalytic performance. However, the high retention of degradation efficiency after 10 cycles suggests that the Pani/rGO@NiFe-DLH composite is quite durable and capable of repeated use, making it a promising candidate for long-term, sustainable photocatalytic applications.

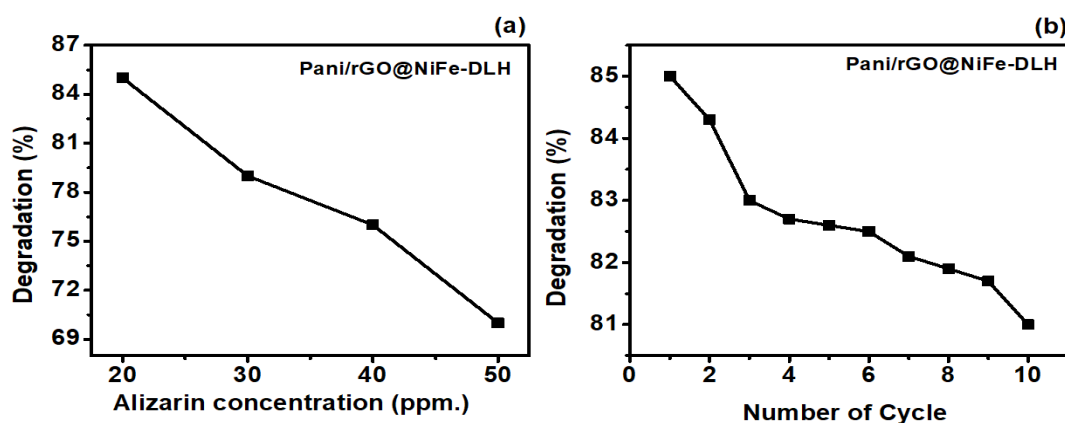


Fig. 6. (a) Concentration dependence and (b) cyclic stability of Pani/rGO@NiFe-DLH catalyst.

3.8. Possible degradation mechanism

When exposed to visible light, the catalyst absorbs photons, which results in the creation of electron-hole pairs and the photocatalytic destruction of AYR. Low photocatalytic activity in pure NiFe-DLH is caused by rapid charge carrier recombination and poor absorption of visible light (Figure 7). The introduction of rGO into NiFe-DLH significantly improves charge separation, as rGO acts as an electron sink, capturing photogenerated electrons and extending the lifetime of reactive species. This enhancement is further amplified in the Pani/rGO@NiFe-DLH composite, where Pani absorbs visible light, transfers photogenerated electrons to rGO, and reduces recombination thus expanding the absorption range into the visible spectrum in an efficient manner. Pani and rGO work in concert to increase electron mobility and promote the production of reactive oxygen species, including hydroxyl radicals ($\cdot\text{OH}$) and superoxide radicals ($\text{O}_2^{\cdot-}$), which mineralizes AYR. Effective interaction between dye molecules and the catalyst's active sites maximize the generation of reactive species, resulting in the maximum degradation efficiency, at an ideal dye concentration of 20 ppm. However, at higher concentrations, the excess dye molecules occupy active sites and absorb incident light, reducing the availability of photons and reactive species, thereby lowering degradation efficiency. The Pani/rGO@NiFe-DLH composite demonstrates excellent stability, retaining substantial photocatalytic activity even after multiple cycles, with only a slight decrease due to surface fouling by degradation intermediates.

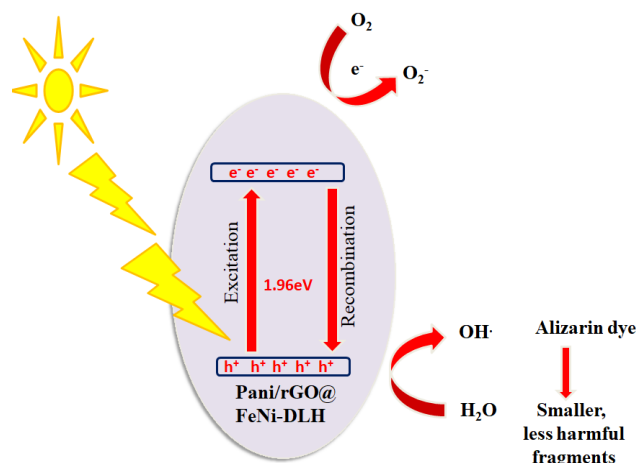


Fig. 7. Proposed degradation mechanism of AYR by Pani/rGO@FeNi-DLH.

4. Analysis of antibacterial properties

4.1. Antimicrobial studies on NiFe-DLH, rGO@NiFe-DLH, and Pani/rGO@NiFe-DLH against *E. coli*

Although it is frequently found in the human gastrointestinal tract, the gram-negative bacterium *E. coli* can also cause extraintestinal diseases. Furthermore, it is well known that *E. coli* can create biofilms on medical equipment, which might result in implant failure. Considering these possible resistances, it is essential that implanted medical devices surfaces successfully stop the growth of microorganisms.

In this study, antimicrobial properties of NiFe-DLH, rGO@NiFe-DLH, and Pani/rGO@NiFe-DLH, using *E. coli* as the test organism was studied. *E. coli* was selected for this study due to its known ability to form biofilms and contribute to nosocomial infections. The growth inhibition of *E. coli* in the presence of these three compounds at three different concentrations (0.25, 0.5, and 1 mg/mL) was measured. The results indicated significant growth inhibition of *E. coli* in liquid culture (Figure 8) and among the tested materials, Pani/rGO@NiFe-DLH showed highest antimicrobial activity, achieving a 70% reduction in bacterial growth at a concentration of 1 mg/mL. In comparison, NiFe-DLH demonstrated the least growth inhibition, at 40%, while rGO@NiFe-DLH exhibited moderate growth inhibition of up to 50% at the same concentrations. When these nanocomposite compounds were applied to growing *E. coli* culture plates, a noticeable zone of growth inhibition was observed after one day of incubation (Figure 8).

4.2. Antimicrobial mechanisms of NiFe-DLH, rGO@NiFe-DLH, and Pani/rGO @ NiFe-DLH against *E. Coli*

- (i) Cell membrane damage via reactive oxygen species (ROS) generation by NiFe-DLH and its composites causes lipid, protein and membranes damage [49,50].
- (ii) Sharp nanostructures of NiFe-DLH material with GO sheets causes physical damage leading to cytoplasmic leakage[49,51–53].
- (iii) Further addition of Pani with nanocomposite materials causes electrostatic interaction and charge transfer as the positively charged Pani in Pani/rGO@NiFe-DLH interacts with oppositely charged *E. Coli* which disturbs membrane potential leading to injury to the cell walls.

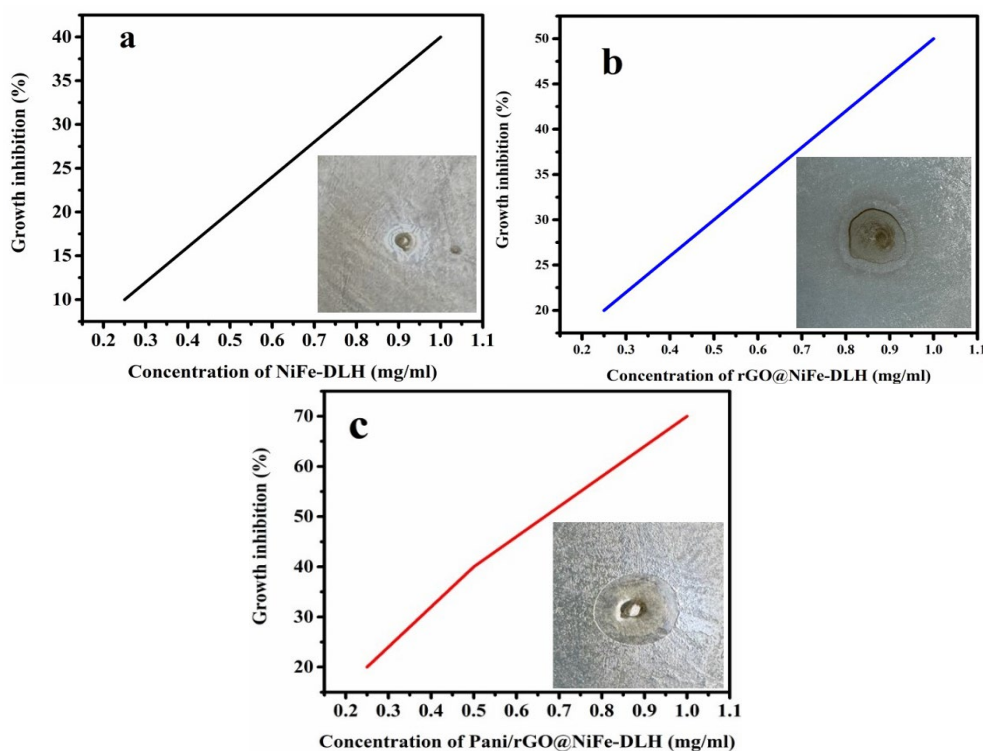


Fig. 8. The antimicrobial study of nanocomposite materials (a) NiFe-DLH (b) rGO@NiFe-DLH, and (c) Pani/rGO@NiFe-DLH, against the *E. coli* as the test organism. The figure indicates the zone inhibition and percent bacterial inhibition at fixed dose 1 mg/mL concentration applied in liquid media.

5. Conclusion

In summary, this work demonstrates that reduced graphene oxide (rGO) and polyaniline (Pani) improves the photocatalytic efficacy of a nickel-iron double layer hydroxide (NiFe-DLH) catalyst. According to photoluminescence (PL) analysis, the addition of rGO to the NiFe-DLH greatly enhanced the photocatalytic degradation of alizarin yellow R (AYR) dye in visible light by encouraging charge separation and lowering recombination. The inclusion of Pani leads to further reduction in that PL intensity and the highest degrading efficiency of 85%, demonstrating the complementary roles of rGO and Pani in lowering recombination and enhancing charge transport. The diffuse reflectance spectroscopy revealed that the Pani/rGO@FeNi-DLH's smaller band gap was linked with increased visible light absorption and photocatalytic activity. After 10 cycles, the composite retained 81% of its original efficiency, demonstrating exceptional reusability. In terms of photocatalytic destruction of organic pollutants, the Pani/rGO@FeNi-DLH composite exhibits high efficiency, stability, and sustainability, indicating considerable promise for environmental applications. The ternary Pani/rGO@FeNi-DLH also showed efficient killing of gram-negative *E. coli* due to the synergistic effect of DLH, rGO and Pani leading to production of reactive oxygen species and disturbing membrane potential of *E. coli*.

Acknowledgments

P. Kumar, one of the authors, expresses gratitude to the Higher Education Department of the Uttar Pradesh, Govt. (India) for providing financial support through the sanction of R & D grant (Letter No. 89/2022/1585/70-4-2022/001-4-32-2022, dated 10/11/2022) and Centre of Excellence (Latter no.78/2024/1015/70-4-2024-001-70-4002(002)/4/2023, dated 23/09/2024). S. Yadav is grateful to the UGC, New Delhi, India, for awarding him the Junior Research Fellowship.

References

- [1] W. U. Khan, S. Ahmed, Y. Dhoble, S. Madhav, *Journal of the Indian Chemical Society* 100, 100829 (2023); <https://doi.org/10.1016/j.jics.2022.100829>
- [2] M. Aslam, M. H. Ali, W. Erum, S. Shehzadi, Z. Khalid, *MARKHOR (The Journal of Zoology)* 09 (2021); <https://doi.org/10.54393/mjz.v2i2.18>
- [3] M. O. Ansari, M. M. Khan, S. A. Ansari, M. H. Cho, *Journal of Saudi Chemical Society* 19, 494 (2015); <https://doi.org/10.1016/j.jscs.2015.06.004>
- [4] J.-Y. Yang, X.-Y. Jiang, F.-P. Jiao, J.-G. Yu, *Applied Surface Science* 436, 198 (2018); <https://doi.org/10.1016/j.apsusc.2017.12.029>
- [5] N. G. Yadav, L. S. Chaudhary, P. A. Sakhare, T. D. Dongale, P. S. Patil, A. D. Sheikh, *Journal of Colloid and Interface Science* 527, 289 (2018); <https://doi.org/10.1016/j.jcis.2018.05.051>
- [6] S. Aghabeygi, M. Khademi-Shamami, *Ultrasonics Sonochemistry* 41, 458 (2018); <https://doi.org/10.1016/j.ultsonch.2017.09.020>
- [7] M. Chethana, L. G. Sorokhaibam, V. M. Bhandari, S. Raja, V. V. Ranade, *ACS Sustainable Chem. Eng.* 4, 2495 (2016); <https://doi.org/10.1021/acssuschemeng.5b01553>
- [8] Z. Zhou, W. Li, J. Song, G. Yi, B. Mei, L. Su, *Ceramics International* 44, 4344 (2018); <https://doi.org/10.1016/j.ceramint.2017.12.028>
- [9] P. Hadi, J. Guo, J. Barford, G. McKay, *Environ. Sci. Technol.* 50, 5041 (2016); <https://doi.org/10.1021/acs.est.6b00021>
- [10] A. Rajeswari, S. Vismaiya, A. Pius, *Chemical Engineering Journal* 313, 928 (2017); <https://doi.org/10.1016/j.cej.2016.10.124>
- [11] E. Brillas, C. A. Martínez-Huitle, *Applied Catalysis B: Environmental* 166-167, 603 (2015); <https://doi.org/10.1016/j.apcatb.2014.11.016>
- [12] S. N. Malik, P. C. Ghosh, A. N. Vaidya, S. N. Mudliar, *Journal of Hazardous Materials* 357, 363 (2018); <https://doi.org/10.1016/j.jhazmat.2018.05.070>
- [13] D. Vidyasagar, S. G. Ghugal, A. Kulkarni, P. Mishra, A. G. Shende, Jagannath, S. S. Umare, R. Sasikala, *Applied Catalysis B: Environmental* 221, 339 (2018); <https://doi.org/10.1016/j.apcatb.2017.09.030>
- [14] A. Bhattacharjee, M. Ahmaruzzaman, *Journal of Colloid and Interface Science* 448, 130 (2015); <https://doi.org/10.1016/j.jcis.2015.01.083>
- [15] J. Zhang, P. Wang, J. Sun, Y. Jin, *ACS Appl. Mater. Interfaces* 6, 19905 (2014); <https://doi.org/10.1021/am505371g>
- [16] P. K. Boruah, B. Sharma, I. Karbhal, M. V. Shelke, M. R. Das, *Journal of Hazardous Materials* 325, 90 (2017); <https://doi.org/10.1016/j.jhazmat.2016.11.023>
- [17] H. Park, H. Kim, G. Moon, and W. Choi, *Energy & Environmental Science* 9, 411 (2016); <https://doi.org/10.1039/C5EE02575C>
- [18] J. Kou, C. Lu, J. Wang, Y. Chen, Z. Xu, R. S. Varma, *Chem. Rev.* 117, 1445 (2017); <https://doi.org/10.1021/acs.chemrev.6b00396>
- [19] M. A. Henderson, I. Lyubnitsky, *Chem. Rev.* 113, 4428 (2013); <https://doi.org/10.1021/cr300315m>
- [20] J. Fei, J. Li, *Adv Mater* 27, 314 (2015); <https://doi.org/10.1002/adma.201404007>
- [21] C. Dong, K.-L. Wu, X.-W. Wei, J. Wang, L. Liu, B.-B. Jiang, *Applied Catalysis A: General* 488, 11 (2014); <https://doi.org/10.1016/j.apcata.2014.09.025>
- [22] Z. Li, M. Shao, L. Zhou, R. Zhang, C. Zhang, J. Han, M. Wei, D. G. Evans, X. Duan, *Nano Energy* 20, 294 (2016); <https://doi.org/10.1016/j.nanoen.2015.12.030>
- [23] S.-J. Xia, F.-X. Liu, Z.-M. Ni, J.-L. Xue, P.-P. Qian, *Journal of Colloid and Interface Science* 405, 195 (2013); <https://doi.org/10.1016/j.jcis.2013.05.064>
- [24] R. Liang, R. Tian, W. Shi, Z. Liu, D. Yan, M. Wei, D. G. Evans, X. Duan, *Chem. Commun.*

- 49, 969 (2013); <https://doi.org/10.1039/C2CC37553B>
- [25] M. Zhang, B. Gao, Y. Yao, M. Inyang, *Chemosphere* 92, 1042 (2013); <https://doi.org/10.1016/j.chemosphere.2013.02.050>
- [26] Q. Liu, J. Ma, K. Wang, T. Feng, M. Peng, Z. Yao, C. Fan, S. Komarneni, *Ceramics International* 43, 5751 (2017); <https://doi.org/10.1016/j.ceramint.2017.01.119>
- [27] Y. Meng, W. Luo, S. Xia, Z. Ni, *Catalysts* 7, 143 (2017); <https://doi.org/10.3390/catal7050143>
- [28] Y. Lu, B. Jiang, L. Fang, F. Ling, J. Gao, F. Wu, X. Zhang, *Chemosphere* 152, 415 (2016); <https://doi.org/10.1016/j.chemosphere.2016.03.015>
- [29] C.-H. Hung, C. Yuan, H.-W. Li, *Journal of Hazardous Materials* 322, 243 (2017); <https://doi.org/10.1016/j.jhazmat.2016.01.073>
- [30] C. B. Hiragond, P. K. Khanna, P. V. More, *Vacuum* 155, 159 (2018); <https://doi.org/10.1016/j.vacuum.2018.06.009>
- [31] Y. Park, A. Numan, N. Ponomarev, J. Iqbal, M. Khalid, *Journal of Environmental Chemical Engineering* 9, 106006 (2021); <https://doi.org/10.1016/j.jece.2021.106006>
- [32] A. Jilani, M. H. D. Othman, M. O. Ansari, I. Ullah Khan, S. Z. Hussain, *Synthetic Metals* 251, 30 (2019); <https://doi.org/10.1016/j.synthmet.2019.03.019>
- [33] L. Li, Y. Yang, Y. Wang, M. Liang, Y. Huang, *Journal of Materials Research and Technology* 9, 5463 (2020); <https://doi.org/10.1016/j.jmrt.2020.03.072>
- [34] D. Xia, L. Zhou, S. Qiao, Y. Zhang, D. Tang, J. Liu, H. Huang, Y. Liu, Z. Kang, *Materials Research Bulletin* 74, 441 (2016); <https://doi.org/10.1016/j.materresbull.2015.11.007>
- [35] C. Xu, X. Wu, J. Zhu, X. Wang, *Carbon* 46, 386 (2008); <https://doi.org/10.1016/j.carbon.2007.11.045>
- [36] H.-B. Pan, C. M. Wai, *J. Phys. Chem. C* 113, 19782 (2009); <https://doi.org/10.1021/jp903799w>
- [37] C. Nethravathi, T. Nisha, N. Ravishankar, C. Shivakumara, M. Rajamathi, *Carbon* 47, 2054 (2009); <https://doi.org/10.1016/j.carbon.2009.03.055>
- [38] A. G. Agrios, P. Pichat, *Journal of Photochemistry and Photobiology A: Chemistry* 180, 130 (2006); <https://doi.org/10.1016/j.jphotochem.2005.10.003>
- [39] A. Jilani, M. O. Ansari, M. Oves, S. Z. Hussain, M. H. D. Othman, in *Modern Age Waste Water Problems : Solutions Using Applied Nanotechnology*, edited by M. Oves, M. O. Ansari, M. Zain Khan, M. Shahadat, and I. M.I. Ismail (Springer International Publishing, Cham, 2020), pp. 329-337; https://doi.org/10.1007/978-3-030-08283-3_16
- [40] O. Długosz, M. Banach, *Solid State Sciences* 149, 107456 (2024); <https://doi.org/10.1016/j.solidstatesciences.2024.107456>
- [41] A. Ali Khan, M. Tahir, N. Khan, *Journal of Energy Chemistry* 84, 242 (2023); <https://doi.org/10.1016/j.jechem.2023.04.049>
- [42] M. Masum Billah, G. Kawamura, *Materials Horizons* (2025).
- [43] H. F. Nassar, H. M. Ahmed, M. E. Fawzy, *Desalination and Water Treatment* 303, 193 (2023); <https://doi.org/10.5004/dwt.2023.29740>
- [44] S. T. Almutairi, *Heliyon* 10, (2024); <https://doi.org/10.1016/j.heliyon.2024.e28900>
- [45] H. Saraee, M. Tanzifi, M. Mansouri, M. Saraee, M. Tavakkoli Yarak, *Environmental Research* 267, 120658 (2025); <https://doi.org/10.1016/j.envres.2024.120658>
- [46] Z. Lin, L. Pei, S. Liu, X. Jiang, W. Xu, F. Li, X. Wu, H. Wang, X. Lu, *Journal of Water Process Engineering* 70, 106909 (2025); <https://doi.org/10.1016/j.jwpe.2024.106909>
- [47] F. Collin, *International Journal of Molecular Sciences* 20, 2407 (2019); <https://doi.org/10.3390/ijms20102407>
- [48] M. F. Hanafi, N. Sapawe, *Materials Today: Proceedings* 31, 318 (2020); <https://doi.org/10.1016/j.matpr.2020.06.066>
- [49] Z. Yu, M. Lepoitevin, C. Serre, *Adv Healthcare Materials* 2402630 (2024).

- [50] S. Rakshit, S. Ghosh, S. Chall, S. S. Mati, S. P. Moulik, S. C. Bhattacharya, RSC Adv. 3, 19348 (2013); <https://doi.org/10.1039/c3ra42628a>
- [51] M. Oves, M. O. Ansari, M. S. Ansari, A. Memić, Molecules 28, 2814 (2023); <https://doi.org/10.3390/molecules28062814>
- [52] A. Pal, S. Bhattacharjee, J. Saha, M. Sarkar, P. Mandal, Critical Reviews in Microbiology 48, 327 (2022); <https://doi.org/10.1080/1040841X.2021.1970512>
- [53] A. Pal, S. Bhattacharjee, J. Saha, M. Sarkar, P. Mandal, Critical Reviews in Microbiology 48, 327 (2022); <https://doi.org/10.1080/1040841X.2021.1970512>